ELSEVIER

Contents lists available at ScienceDirect

# International Journal of Non-Linear Mechanics

journal homepage: www.elsevier.com/locate/nlm





# A new constitutive relation to describe the response of bones

J. Arumugam <sup>a</sup>, P. Alagappan <sup>a</sup>, J. Bird <sup>b</sup>, M. Moreno <sup>c</sup>, K.R. Rajagopal <sup>c,\*</sup>

- <sup>a</sup> Department of Civil Engineering at IIT Madras, India
- <sup>b</sup> M.D. Anderson Cancer Center, United States of America
- <sup>c</sup> Department of Mechanical Engineering at Texas A&M University, United States of America

#### ARTICLE INFO

Keywords:
Porous elastic solid
Implicit constitutive relation
Bone model
Density dependent material moduli
Inhomogeneous elastic solid
Stress concentration

#### ABSTRACT

Trabecular bone, a solid that has a heterogeneous porous structure, demonstrates nonlinear stress–strain relationship, even within the small strain region, when subject to stresses. It also exhibits different responses when subject to tension and compression. This study presents the development of an implicit constitutive relation between the stress and the linearized strain specifically tailored for trabecular bone-like materials. The structure of the constitutive relation requires the solution of the balance of linear momentum and the constitutive relations simultaneously, and in view of this, a two-field mixed finite element model capable of solving general boundary value problems governed by a system of coupled equations is proposed. We investigate the effects of nonlinearity and heterogeneity in a dogbone-shaped sample. Our study is able to capture the significant nonlinear characteristics of the response of the trabecular bone undergoing small strains in experiments, in both tension and compression, very well.

#### 1. Introduction

The mechanical properties of bone, such as stiffness, are greatly influenced by natural variations in the porosity of the bone, and hence its density. The papers that address this issue are too numerous to cite and so we shall selectively cite a few of them see [1-5] with a clear caveat that this is just a very small representative sample. Not only does the porosity of the bone affect the mechanical properties of the bone, it affects the permeability of the bone and governs the nature of the interstitial flow within the bone (see [6]). It is also well-known that bone is viscoelastic (see [7-9]) and its viscoelastic nature might even depend on the gender (see [10]), and it is also well recognized that the trabecular bone is anisotropic, usually assumed to be transversely isotropic (see [11–15]). However, to incorporate the fact that the bone is porous and hence its properties depend on the density and the applied pressure, that it is viscoelastic, anisotropic, inhomogeneous, and that its response is distinct in tension versus compression, all at one go, is a tall order. In view of this, in this study we restrict our modeling of the bone to being elastic, and that it exhibits nonlinear response in the small strain range, and displays distinct behavior in tension and compression. We do caution that this is an approximation and that the nonlinearity in the response might be due to progression of damage. Moreover, data is not available with regard to unloading and hence we are not in a position to fashion a model that can capture the dissipation that might be generated. We are essentially assuming this dissipation is

negligible and the bone is elastic, the anisotropy and viscoelastic nature of bone will be the subject matter of subsequent study.

Trabecular bone, a porous material found in the human skeletal system, exhibits complex mechanical behavior. For trabecular bone the relationship between the stress and the strain is nonlinear, even under small strains (see [16]). Furthermore, the response during tension differs from the response during compression. Understanding and accurately modeling the mechanical response of trabecular bone is crucial for design and analysis in orthopedics, and tissue engineering. Consequently, there is a need to develop appropriate constitutive relations and appropriate computational tools that can capture the unique mechanical properties of this material.

Accurate mechanical modeling of bone behavior has significant clinical application, particularly in guiding patient-specific orthopedic care. Understanding this behavior would greatly improve numerous clinical challenges such as fracture risk assessment, reconstructive implant selection, physical therapy strategy, and activity recommendations. Advances in imaging resolution and computational power have made CT-based finite element analysis (FEA) increasingly viable for regular clinical use (see [17–19]). FEA-based fracture prediction of metastatic bone have shown promising results, indicating computational predictive accuracy comparable to experienced orthopedic surgeons (see [20]). Comprehensive models of bone fracture healing require integration of cellular response to mechanostimulation as tissue differentiation within the fracture callus is widely understood to

E-mail address: krajagopal@tamu.edu (K.R. Rajagopal).

<sup>\*</sup> Corresponding author.

be regulated by the distribution of local strain (see [21]). Despite some success, many of these computational models are predicated on isotropic and/or linear constitutive models of the bone which do not capture the complexity of the tissue's mechanical response.

Bone presents interesting challenges to the constitutive modeler. As mentioned earlier unlike most metals and polymers, the material moduli characterizing the bone's response in tension differs from that during compression, even when the deformations are small. Such behavior is also exhibited by materials such as rocks, and is a consequence of the material's internal structure. Given the dependence of the material moduli on the density, we are able to capture such response characteristics by allowing the material moduli to depend on the magnitude of the trace of the linearized strain which in virtue of the balance of mass is related to the density, the details of which are provided later.

In this study, we focus on developing an implicit constitutive relation for trabecular bone-like materials. Unlike the traditional linearized elastic model, which assumes a linear relationship between the stress and strain, trabecular bone demonstrates nonlinear behavior, particularly in the small strain region, even when strains are below 3%. This nonlinear stress–strain relationship arises due to the intricate architecture and porous nature of trabecular bone, which affects its mechanical response under external loading conditions.

We use a two-field mixed finite element model capable of solving general boundary value problems associated with the equilibrium of elastic bodies that are described by implicit equations. This approach enables us to accurately represent the mechanical response of trabecular bone-like materials under diverse loading conditions. Specifically, we will examine a dogbone-shaped sample of a trabecular bone subjected to simple compression and compare the resulting stresses and strains to those obtained from the classical linearized elastic solid.

#### 2. Implicit constitutive relation for trabecular bone

# 2.1. Preliminaries

Consider an abstract body B occupying a region  $\Omega_R$  in three-dimensional Euclidean space, with boundary  $\partial\Omega_R$ . The body's particles are labeled by their material positions X at a conveniently chosen reference configuration, preferably, at time t=0. Let N(X) denote the outward unit normal to the boundary of the body at X. As the body deforms in time due to forces acting on it, let it occupy a different region  $\Omega_t$  in space, the positions x of the particles in this configuration of the body are related to their initial positions through a differentiable map  $x=\chi(X,t)$  referred to as the motion of the body. We can now define the displacement field u=x-X, the deformation gradient  $F=\frac{\partial \chi}{\partial X}$ , the right Cauchy–Green tensor  $C=F^TF$ , the left Cauchy–Green tensor  $B=FF^T$ , and Green–Saint Venant strain tensor E=1/2(C-I), associated with the motion.

Denoting the density of the body in the reference configuration and configuration at time t as  $\rho_R$  and  $\rho$ , respectively, the balance of mass is

$$\rho_R = \rho \ det F. \tag{1}$$

We restrict ourselves to deformations that satisfy  $J=\det F>0$ . Denoting the first Piola–Kirchhoff and Cauchy stress tensors by S and

T (where  $S = JTF^{-T}$ ,) respectively, the balance of linear momentum under static equilibrium is

$$\mathbf{0} = Div \ \mathbf{S} + \mathbf{f}, \quad in \ \Omega_R \tag{2}$$

where f are body forces per unit volume in the reference configuration and Div is divergence operator with respect to X.

The linearized strain tensor is defined as:

$$\epsilon(\mathbf{u}) = \frac{1}{2} \left( \frac{\partial \mathbf{u}}{\partial \mathbf{X}} + \frac{\partial \mathbf{u}}{\partial \mathbf{X}}^T \right). \tag{3}$$

As we shall be restricting ourselves to small strains, we do not further distinguish between S and T.<sup>2</sup> The balance of angular momentum implies  $T = T^T$ .

Eq. (2) is the governing equation for static boundary value problems along with boundary conditions

$$TN = g \quad on \ \Gamma_N$$
 (4)

$$u = u_D$$
 on  $\Gamma_D$  (5)

where g and  $u_D$  are prescribed boundary traction and displacements<sup>3</sup>;  $\partial \Omega_R = \Gamma_N \cup \Gamma_D$  and  $\Gamma_N \cap \Gamma_D$  is a null set.

Displacement field that satisfies (2) along with boundary conditions (4) and (5) cannot be solved for unless the constitutive relation between stress T and  $\epsilon$  (Eq. (3)) is further prescribed. Balance of mass implies  $\rho \approx \rho_R (1-tr\epsilon)$  and needs to be appropriately enforced. Balance of angular momentum is enforced by the requirement that the stress be symmetric, i.e.,  $T = T^T$ .

#### 2.2. Implicit constitutive relations

Within the context of small deformation gradients, and hence small strains, general constitutive relations for Cauchy elastic bodies [28,29], and hence Green elastic bodies [30] reduce to the classical linearized elastic constitutive relation which is characterized by two constants, the two Lame' constants or alternatively by the Young's modulus and Poisson's ratio. The material moduli have to be constants and cannot depend on density in virtue of the balance of mass (see [31]). Since we are interested in describing bodies whose material constants depend on density, even when they are subject to small strains, we cannot consider linearizations of Cauchy elastic bodies. The way out of this impasse is to consider the linearization of the more general class of elastic bodies introduced by [32] wherein the stress and the Cauchy–Green tensor are related through an implicit relation.

Linearizing such an implicit relation under the assumption that the displacement gradient is small leads to a nonlinear implicit relation

$$\lambda_i tr \epsilon \approx \lambda_i \left( \frac{\rho - \rho_R}{\rho_R} \right), \quad i=1, 2, 3.$$

<sup>3</sup> Though we prescribe the displacement at the boundary, we recognize that this displacement is a consequence of the appropriate traction at the boundary. Boundary conditions are a consequence of the nature of the material on either side of the boundary and how the body and its surroundings interact. Forces are exerted at the boundary of the body of interest and the body deforms leading to a displacement of the boundary. Since in some instances, we are not able to measure the cause (in this case the forces at the boundary) but can easily ascertain the displacement or velocity (the effect), we prescribe the latter.

<sup>&</sup>lt;sup>1</sup> It has been well established that rocks exhibit different response characteristics in tension and compression (see [22–25]) and such a response is attributed to the nature of the porous structure of the rocks (see [26]). [27] have developed an implicit constitutive relation to describe the response of such rocks. Their constitutive relation expresses the linearized strain as a nonlinear function of the stress, a constitutive relation that can be obtained by linearizing an appropriate implicit constitutive relation between the stress and the Cauchy–Green strain.

<sup>&</sup>lt;sup>2</sup> Since the norm of the displacement gradient is of  $\mathcal{O}(\delta)$ ,  $\delta \ll 1$ , the Cauchy stress  $T \approx S$  (Piola–Kirchhoff stress). This is a consequence of  $\det F \approx (1+tr(\nabla u))$  and  $F^{-T}=(1+\nabla u)^{-T}\approx (1-\nabla u)^T$ . The assumption is the same as that which is made in the classical theory of linearized elasticity. While in comparison to 1,  $tr(\nabla u)$  is of  $\mathcal{O}(\delta)$  and is ignored, the term  $\lambda_i tr(\nabla u)$  cannot be ignored as  $\lambda_i$ , i=1,2,3 (see Eq. (6) that follows), is large. Under the assumption of small displacement gradient, the balance of mass approximates to  $\rho \approx \rho_R (1-tr(\nabla u))$ . Once again, since the norm of the displacement gradient is small, while the reference and current densities will be approximately the same, the term

between the Cauchy stress and the linearized strain. At times such a relation can be simplified to express the stress in terms of the linearized strain wherein nonlinear terms of the linearized strain appear, but such a form of expressing the constitutive relation is not allowable as nonlinear terms in the linearized strain are to be ignored with regard to the linearized strain. As shown by [33], linearizing an implicit elastic body and inverting the expression, and inverting the expression for the stress in terms of the Cauchy–Green strain and then inverting do not lead to the same constitutive relation. Thus, one has to restrict oneself to solving the system of equations consisting in the balance of linear momentum and the constitutive relation simultaneously. This requires the development of non-standard numerical techniques to solve boundary value problems. In this study, we develop a finite element method to analyze the problem.

We study several boundary value problems. We compare identical two dogbone samples, when both of them are homogeneous, both of them have an inclusion that is of lower and higher density, and thus softer and stiffer, respectively, in a small region of the dog bone than the rest, the inhomogeneities being in different locations. We also study the problem of a hole and a semicircular notch in the dog bone. As is to be expected, in the region with lower density and less stiffness we obtain strains that are much higher than the rest of the body. The linearized elastic body has constant density and thus constant Young's modulus. (Of course, we can have an inhomogeneous linearized elastic body whose Young's modulus varies over the body. However, the Young's modulus cannot depend on the density as this would immediately imply that the density depends on tre, and the constitutive relation would no more be linear in the linearized strain.)

#### 2.3. Density-dependent constitutive relations

We shall consider a sub-class of the linearization of the implicit relations considered by [34,35], specifically one wherein the Cauchy stress and the linearized strain appear linearly. Though the stress and strain appear linearly in the implicit relation, the relation is not bilinear. This allows the constitutive relation to capture the nonlinear response exhibited by the Trabecular bone while undergoing small strain (see Fig. 1).

We consider an implicit equation of the form [31]:

$$(1 + \lambda_1(trT))\epsilon - B_1(1 + \lambda_2(tr\epsilon))T - B_2(1 + \lambda_3(tr\epsilon))(trT)I = 0.$$
 (6)

Note that in Eq. (6) only a linear term in  $\epsilon$  appears. It is shown in footnote 2, since  $tr\epsilon$  is linearly related to the density, density appears only linearly in the constitutive relation. The Young's modulus is usually assumed to be a power-law of the density. Such an assumption is totally ad hoc in that it will not arise as a proper linearization of Cauchy elastic bodies or even implicit elastic bodies as this would imply the constitutive relation will not be linear in  $\epsilon$ . For instance, in the paper by [36], in addition to the constitutive relation (6) wherein  $tr\epsilon$  appears linearly, they use the generalization of the Young's modulus dependent on a power-law for the density. However, such an assumption is not consistent with requiring that only a linear expression of  $tr\epsilon$  is to appear in the constitutive relation. With regard to the corroboration of the results of the experiment under consideration the choice of constitutive relation (6) wherein  $tr\epsilon$  appears linearly seems to suffice.

In view of the balance of mass, the term  $tr\epsilon$  can be expressed in terms of the current density and the reference density. Since trT is the mean value of the stress,<sup>4</sup> the material moduli depend on both density and the mean value of the stress, which is an expected characteristic of porous solids.

Table 1
Parameters values in constitutive relation (8) calibrated for trabecular bone data in Fig. 1.

$\lambda_1$ (MPa <sup>-1</sup> )	$\lambda_2 = -\lambda_3 = \gamma$ (no units)	E (MPa)	ν (no units)	$B_1$ (MPa <sup>-1</sup> )	$\begin{array}{c} B_2 \\ (\text{MPa}^{-1}) \end{array}$
0.	35.	200.	0.3	(1+v)/E	-v/E

We notice that when  $\lambda_1$ ,  $\lambda_2$  and  $\lambda_3$  are zero, the constitutive relation reduces to that for a classical linearized elastic solid. The constitutive relation (6) when  $\lambda_1$  is zero has been studied recently by Murru et al. [38–41], and a further simplification of the constitutive relation by thresholding has been carried out by Itou et al. [42–44].

#### 2.4. Constitutive relation for trabecular bone

For the material described by the constitutive relation (6) one can define, when  $\lambda_1 = 0$ , a generalized Young's modulus through<sup>5</sup>

$$E_g = \frac{1}{B_1[1 + \lambda_2 t r \epsilon] + B_2[1 + \lambda_3 t r \epsilon]}.$$
 (7)

The generalized Young's modulus of trabecular bone decreases during both compression and extension, which would not be captured by the above expressions for the generalized Young's modulus. We thus modify our constitutive relation to the following expression that is in keeping with the fact that the Young's modulus decreases during both extension and compression:

$$(1 + \lambda_1(trT))\epsilon - B_1(1 + \lambda_2|tr\epsilon|)T - B_2(1 + \lambda_3|tr\epsilon|)(trT)I = 0.$$
 (8)

where |.| denotes absolute value. While the constitutive relation (6) could lead to a generalized Young's modulus that decreases during both compression and tension if different parameters for  $\lambda_i$ , i=1,2,3 are chosen differently for tension and compression, the constitutive relation (8) can describe the same response using the same parameter values in compression and tension.

To simulate the response of a dogbone shaped sample of a trabecular bone under tension, we employed the parameters listed in Table 1. The normal values were obtained by fitting the model with the experimental data for tension of the trabecular bone sourced from [45]. These values were used to fit the compressive response which is different from that in tension. That is, the material moduli determined by fitting tension were able to predict the response in compression. The Young's modulus E and Poisson's ratio  $\nu$  used to compute the material constants  $B_1$  and  $B_2$  correspond to the values appropriate for the classical linearized elastic response.

Rewriting the generalized modulus for the constitutive relation (8) using the chosen form for  $B_1$  and  $B_2$  in Table 1,

$$E_g = \frac{E}{1 + [\lambda_2 + \nu(\lambda_2 - \lambda_3)]|tr\epsilon|}.$$
 (9)

We have set  $\lambda_1 = 0$  and  $\lambda_2 = -\lambda_3 = \gamma$  in order to minimize both the number of parameters used as well the magnitude of the parameters.<sup>6</sup>

<sup>&</sup>lt;sup>4</sup> The term pressure is used rather indiscriminately in mechanics and especially in incompressible nonlinear materials, the Lagrange multiplier that enforces the constraint of incompressibility is incorrectly referred to as the pressure (see [37] for a discussion of the notion of pressure in mechanics).

 $<sup>^5</sup>$  There is a typographical error in [31], it should be  $\lambda_2$  and  $\lambda_3$  as in the equation above and not  $\lambda_1$  and  $\lambda_2$  as it appears in [31]. The generalized Young's modulus defined in (7) depends inversely on the trace of the linearized strain and since the  $tre \approx \left(\frac{\rho-\rho_R}{\rho_R}\right)$ , it depends inversely on the density. Usually, one assumes a power-law dependence for the generalized Young's modulus for the density and this would imply that trace of the linearized strain would appear in a nonlinear fashion in the constitutive relation. For instance, such a choice was made to study the deformation of beams within the context of the constitutive relation studied in this paper by [46]. Here, we are interested in investigating the consequences of assuming that the trace of the linearized strain appears linearly in the constitutive theory.

<sup>&</sup>lt;sup>6</sup> When calibrating a suitably selected constitutive relation using experimental data that may possess noise and bias, the selection of a model containing

#### Bone Stress-Strain Relationship Calibration

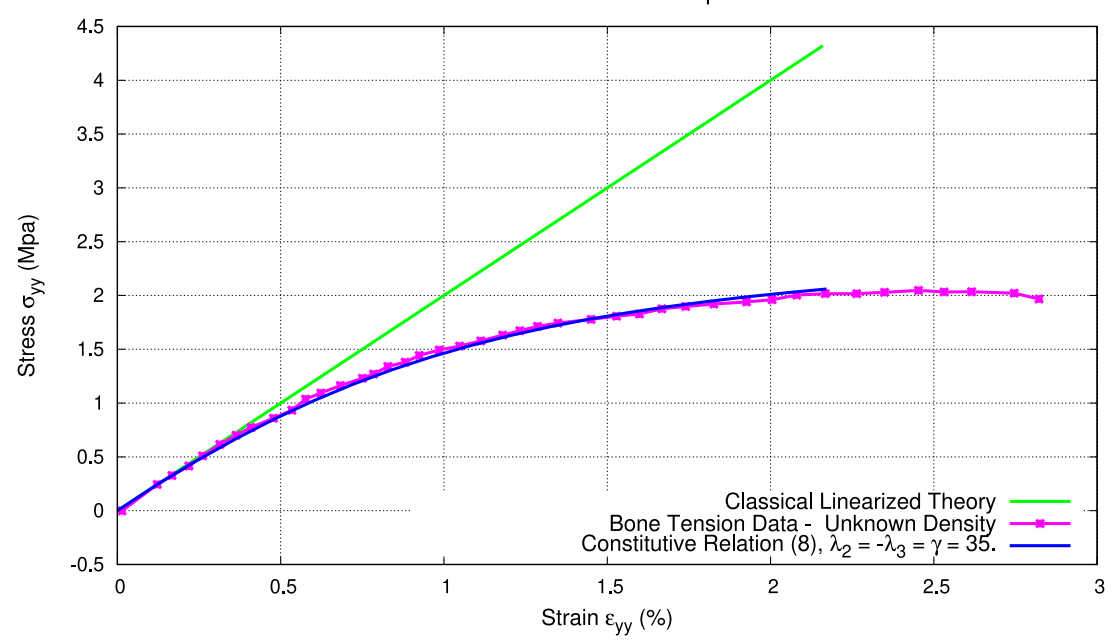


Fig. 1. Comparison of experimental data with results from the linear and nonlinear models for trabecular bone in tension. Experimental data sourced from [45] are depicted. The maximal stresses in the nonlinear material are approximately 40% lower compared to those in the linear material.

Moreover, during the calibration process of the constitutive relation with experimental data, a deliberate effort was made to decrease both the  $L_0$  and  $L_1$  norms (total number of nonzero elements and sum of the magnitude, respectively) of the parameters.

Fig. 1 presents a comparison between the experimental data and the nonlinear elastic model, utilizing the parameter values listed in Table 1. For the linearized elastic model, we set the parameters  $\lambda_1$ ,  $\lambda_2$ , and  $\lambda_3$  to zero. The figure provides clear evidence of the nonlinear behavior exhibited by trabecular bone, particularly at small strains. The modulus gradually decreases until reaching a strain of 2.5%. Beyond this point, the experimental data indicate signs of material failure and data beyond the failure point are not included in the figure. We notice that at a strain of 2.5%, the predictions of the classical linearized elastic constitutive relation are off by as much as 40%, on the other hand, the constitutive relation (8) provides very good agreement with experimental data. So far we have used one experimental curve (in tension) and fit the parameter  $\gamma$ . We use this same value of  $\gamma$  to predict the response in compression and once again we find excellent agreement with the experimental data (see Fig. 2).

# 2.5. Relation between E and $\rho_R$ for human vertebral bone

In order to model the inhomogeneity due to variations in the reference density, following [47,48], the relation between Young's modulus and reference density is expressed as

$$E(\rho_R(\mathbf{X})) = 2210 \ \rho_R(\mathbf{X}) \tag{10}$$

where  $\rho_R$  (g/cc) is apparent density in reference configuration and E is in MPa. While any inhomogeneity could be directly expressed in terms of Young's modulus E(X), expressing E(X) in terms of  $\rho_R(X)$  allows for the determination of  $\rho_R(X)$  (and in turn E(X)) from clinical and experimental images of bone. Eq. (10) is a statistical regression fit for

human vertebral bone data. In the regression fit, there is significant variation or scatter in E for a given  $\rho_R$  ( $r^2=0.62$ , 41 data samples). Accordingly, the predictions are expected to match for a group of human vertebral bone samples in an average sense rather than for each sample individually. Moreover, the reference density for experimental data in Fig. 1 is not known. In Table 1, we have fit E=200 MPa, corresponding to an apparent density of 0.09 g/cc (based on relation (10)).

Stress-strain relationship, in both tension and compression, predicted by the constitutive relation (8) for different apparent densities (relation (10)) is shown in Fig. 2. By design, stress-strain relation based on constitutive relation (8) displays decrease in modulus for both tension and compression. While there seems to be good agreement with regard to experimental data as evidenced in Figs. 1 and 2 for this specific boundary value problem, it is necessary to validate the constitutive relation under consideration of a sequence of boundary value problems in order to ascertain the efficacy and robustness of the constitutive relation.

We solve a series of boundary value problems involving inclusions, holes and notches to determine if the results make qualitative sense from a physical viewpoint. But this will not suffice, we need to systematically solve boundary value problems that can be corroborated against experiments that can be performed.

#### 3. Finite element formulation

# 3.1. Some preliminary numerical considerations

Consider a domain  $\Omega_R\subset\mathbb{R}^d$  with boundary  $\partial\Omega_R$ . Let the displacement field u in the body correspond to body force f and boundary traction Tn=g acting over a boundary  $\Gamma_N$ . Displacements are specified on the remaining portion of the boundary, i.e.,  $u=u_D$  on  $\Gamma_D=\partial\Omega_R-\Gamma_N$ .

In the finite element method, we seek to find approximate solutions of the static equilibrium equations  $u \in H^1(\Omega)$ , such that the equation

$$\int_{\Omega} T(\mathbf{u}) \cdot \epsilon(\mathbf{v}) \ dV - \int_{\Omega} \mathbf{f} \cdot \mathbf{v} \ dV - \int_{\Gamma_N} \mathbf{g} \cdot \mathbf{v} \ dS = 0$$
 (11)

a minimal number of parameters can be seen as a twofold objective: first, to reduce the discrepancy between the observed data and the predictions generated by the model, and second, to simultaneously minimize the norms of these parameters.

## Bone Stress-Strain Relationship Prediction

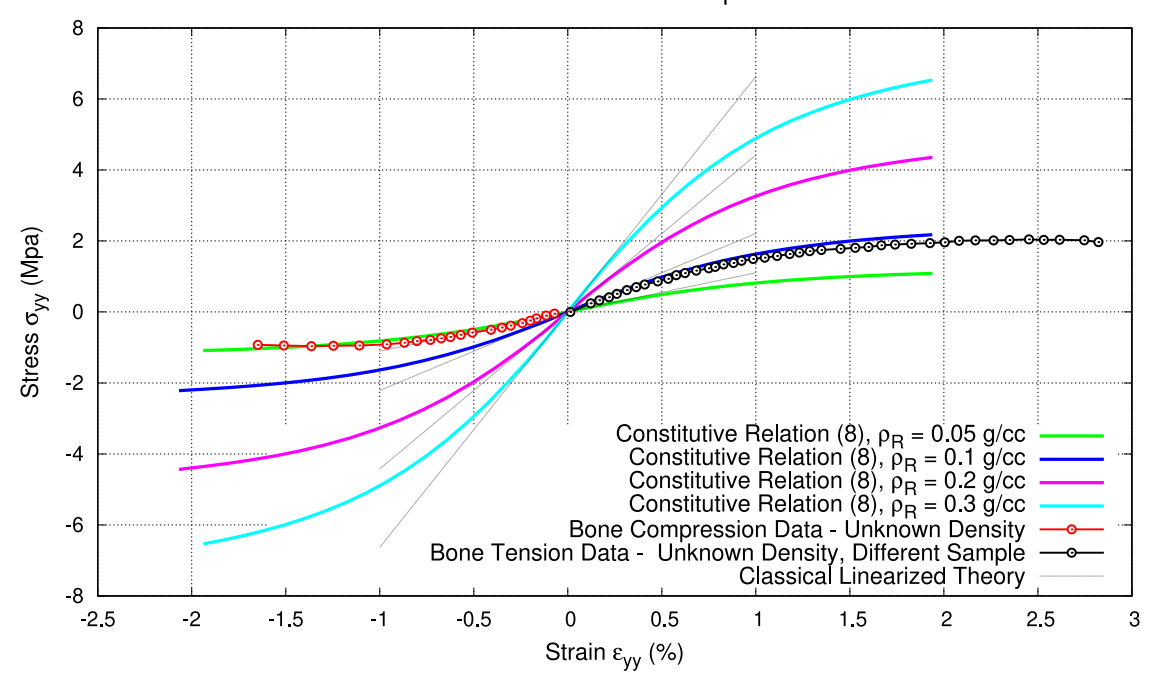


Fig. 2. Model prediction.

is satisfied for all test functions  $v \in H^1(\Omega)$  satisfying the displacement boundary condition on  $\Gamma_D$ . Typically, a Galerkin FE discretization with piecewise quadratic element for the spatial approximation of displacements u is used (see [46] for example).

The linearized strain  $\epsilon(v)^7$  in Eq. (11) is defined through Eq. (3). In such formulation, it is necessary to express stress T explicitly in terms of  $\epsilon(u)$ . In this study, we directly solve Eq. (8) in a weak sense using a mixed two-field formulation.

#### 3.2. Mixed two-field finite element formulation

Consider a domain  $\Omega_R \subset \mathbb{R}^d$  with boundary  $\partial \Omega_R$ . Let the displacement field u in the body correspond to body force f and boundary traction Tn = g acting over a boundary  $\Gamma_N$ . Displacements are specified on the remaining portion of the boundary, i.e.,  $u = u_D$  on  $\Gamma_D =$  $\partial\Omega_R - \Gamma_N$ .

Writing Eq. (8) in the form  $\mathcal{F}(\tau, \epsilon) = 0$ , approximate solutions of the static equilibrium equations are obtained using the finite element method. Specifically, we seek to find doublets  $u \in H^1(\Omega)$  and  $\tau \in$  $H^0(\Omega)$  such that the equations:

$$\int_{\Omega} \mathcal{F}(\tau, \epsilon(u)) \cdot \tau_t \ dV = 0 \tag{12}$$

$$\int_{\Omega} \mathcal{F}(\tau, \epsilon(u)) \cdot \tau_{t} \, dV = 0 \tag{12}$$

$$\int_{\Omega} \tau \cdot \epsilon(v) \, dV - \int_{\Omega} f \cdot v \, dV - \int_{\Gamma_{N}} g \cdot v \, dS = 0 \tag{13}$$

are satisfied for all test functions  $v \in H^1(\Omega)$  satisfying displacement boundary condition on  $\Gamma_D$  and  $\tau_t \in H^0(\Omega)$ .

The geometry was meshed with tetrahedral elements. We used a Galerkin FE discretization with piecewise linear elements for the spatial approximation of displacements u and discontinuous Galerkin elements to approximate  $\tau$ . Additionally, constraints were applied to prevent rigid body motion. Automatic differentiation tools from FEniCS [49]

were used for computational implementation. For plotting the results, solutions were projected onto piecewise linear elements.

The results were cross-validated against test cases from both a prior FEniCS implementation by [46] and an in-house Abaqus implementation. Mesh size was selected to ensure that results remained stable to within a 0.5% margin. Regions near inhomogeneities, holes, and notches were further refined. The largest mesh sizes employed were on the order of 0.3 mm, a scale similar to the typical pixel size of 0.36 mm in clinical CT images (as seen in, for instance, [11]). Further numerical investigations are warranted to comprehensively address convergence

After verifying the computational procedure, we study many boundary value problems involving simple compression of a dogbone shaped sample.

#### 4. Illustrative boundary value problems

We investigate a dogbone shaped sample of length 20 mm (along the y-direction) and thickness of 1 mm. The sample has a width of 5 mm at the ends and 4 mm at the center, as illustrated in Fig. 3(a). In our simulations, the body is centered at the origin, the body force fwas set to zero, and displacement boundary conditions are prescribed on the top and bottom surfaces ( $S_{top}$  and  $S_{bottom}$ ) in the y-direction. Lateral displacements are left unconstrained on the top and bottom surfaces. Rest of the lateral surfaces ( $S_{lateral}$ ) of the body are traction free.8 Specifically,

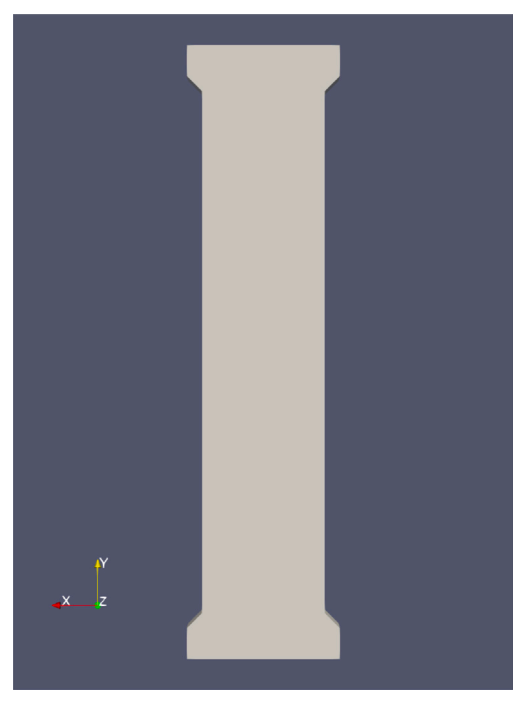
$$[\boldsymbol{u}]_{y} = [\boldsymbol{u}_{D}]_{y}$$
 on surface  $S_{top}, S_{bottom}$  (14)

$$[TN]_x = 0$$
 on surface  $S_{top}, S_{bottom}$  (15)

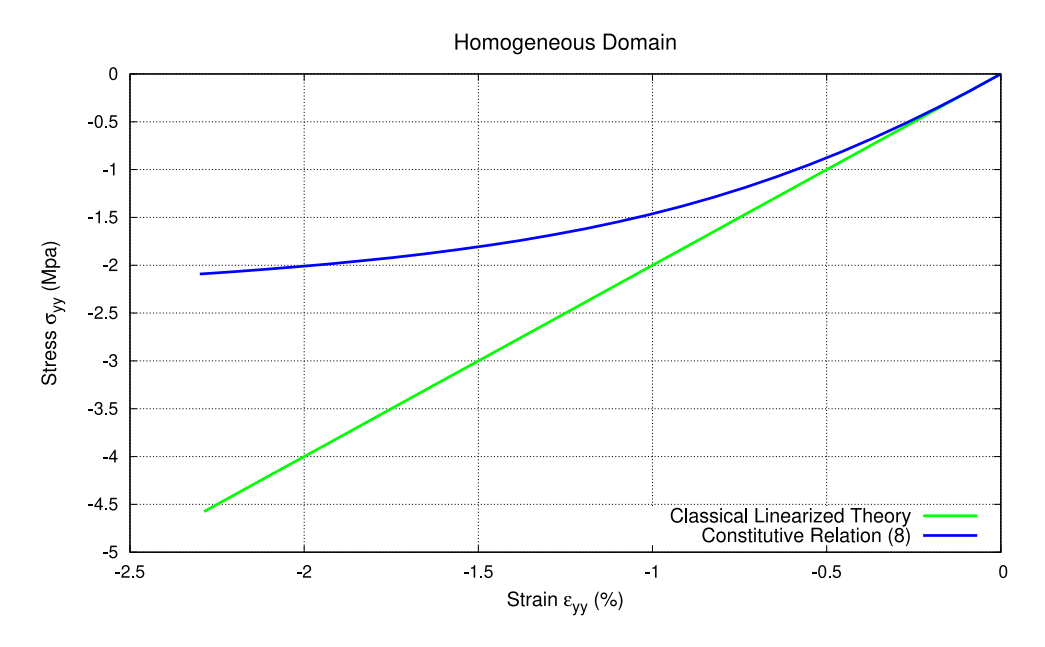
$$[TN]_z = 0$$
 on surface  $S_{top}$ ,  $S_{bottom}$  (16)

<sup>&</sup>lt;sup>7</sup> Balance of angular momentum is enforced in the use of symmetric strain tensor  $\epsilon(v)$  as a test function, instead of the gradient of v as a test function, for stress

<sup>&</sup>lt;sup>8</sup> Enforcing this is not as straightforward as shown here if the problem were solved in Eulerian coordinates as typically done for problems in fluid mechanics (see [50], for example). Enforcing this is also not straightforward if mean value of stress is introduced as a new variable as done in case of some Mixed Three-Field formulations.



(a) Homogeneous dogbone sample.



(b) Comparison of results between the linearized elastic body and the body described by constitutive relation (8).

Fig. 3. Results for homogeneous domain.

 $[TN]_x = 0$  on surface  $S_{lateral}$  (17)

$$[TN]_{v} = 0$$
 on surface  $S_{lateral}$  (18)

$$[TN]_z = 0$$
 on surface  $S_{lateral}$  (19)

To ensure meaningful comparisons of the response of the classical linearized theory and constitutive relation (8), we maintained the same boundary conditions for both the cases. Specifically,  $[u_D]_y$  was set to be 2.25E–4 (m) with appropriate sign on top and bottom surfaces corresponding to a global strain of 2.25% in the longitudinal direction in all cases except for the cases where strains produced by the above displacement were too high thereby possibly violating the small strain

restriction. For the cases with a hole or a notch,  $[u_D]_y$  was set to be 0.75E-4 (m) at the top and bottom surfaces. For the cases with a weaker lateral square inclusion,  $[u_D]_y$  was set to be 1.875E-4 (m) at the top and bottom surfaces.

## 4.1. Homogeneous dogbone sample

Compression results for a representative point from the homogeneous dogbone sample is shown in Figs. 3(b) and 4. We notice a stark distinction between the response of the linearized elastic body and the porous body that is described by the constitutive relation (8), far less

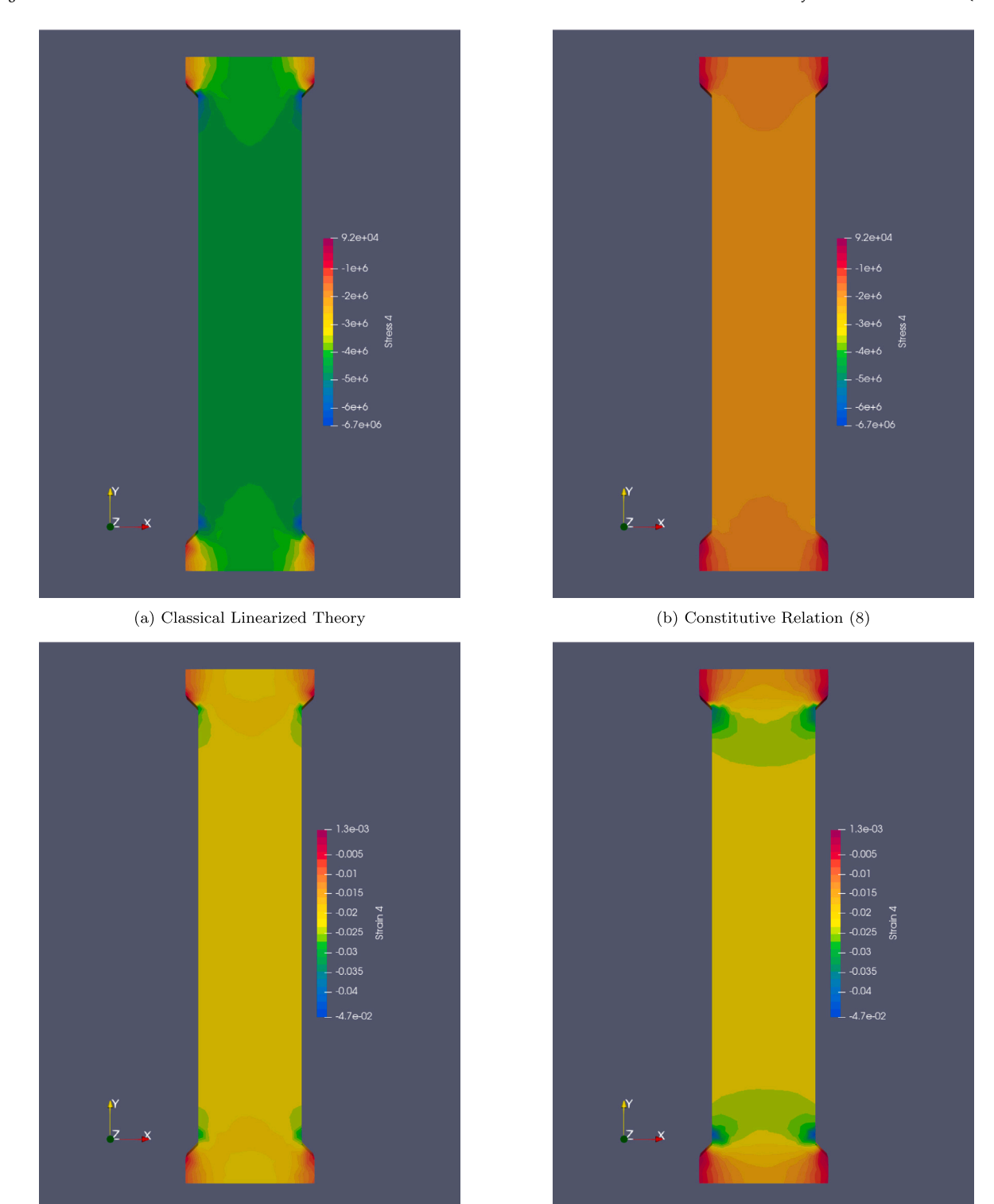


Fig. 4. Comparison of stress field  $\sigma_{yy}$  (top row) and  $\epsilon_{yy}$  (bottom row) for the two cases. Prescribed displacement boundary condition is the same in both the cases.

stress is required to produce the same strain (that is, the porous body becomes softer as it deforms).

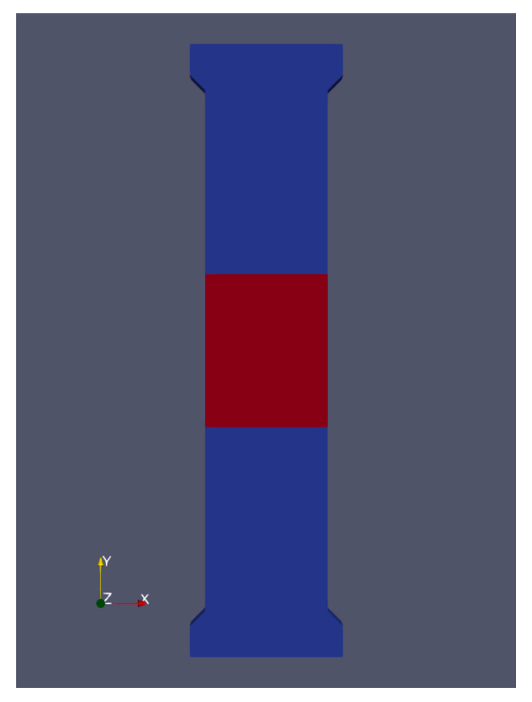
(c) Classical Linearized Theory

## 4.2. Inhomogeneous dogbone samples

To examine the impact of location of the inhomogeneity (in this case location of different density) on the damage/failure of the dogbone

sample, we employed identical geometries featuring different inhomogeneous regions as illustrated in Figs. 5(a) (inhomogeneity in the center of the dogbone), 7(a) (less dense central square inclusion), 9(a) (less dense lateral square inclusion), 11(a) (denser circular inclusion), 13(a) (denser semi-circular lateral inclusion), 15(a) (central hole), and 17(a) (lateral notch). Modulus values along with corresponding reference density values for different types of inhomogeneties are shown in Table 2.

(d) Constitutive Relation (8)



(a) Inhomogeneous domain.

# Inhomogeneity in the Central Region (10% Less Dense)

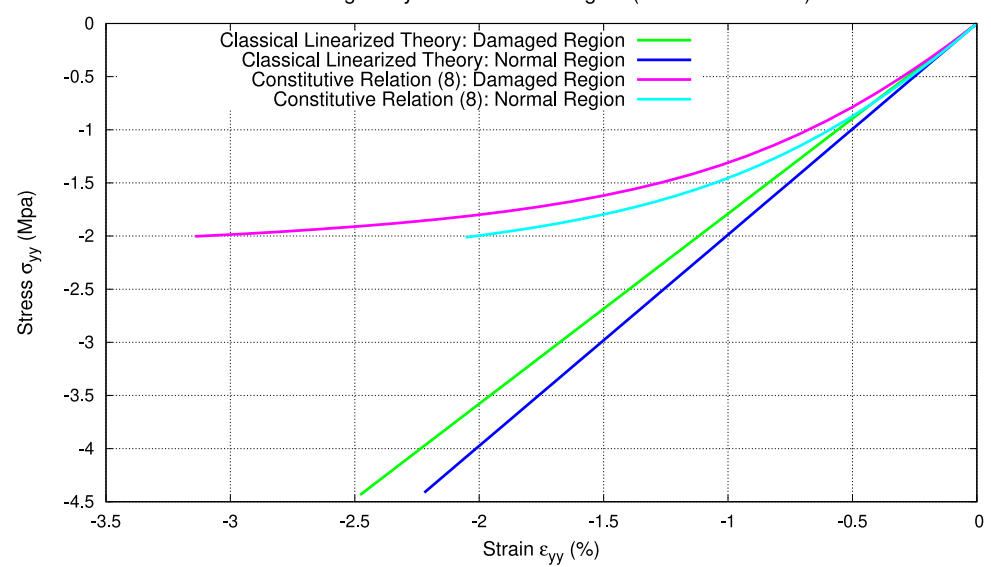


Fig. 5. Inhomogeneity in the center of the dogbone.

Table 2
Reference density values used for various simulation cases.

Parameter	Normal value	Lower density Inclusion 1	Lower density Inclusion 2	Higher density Inclusion
E (MPa)	200	180	100	300
Corresponding $\rho_R$ from relation (10) (g/cc)	0.09	0.08	0.045	0.14

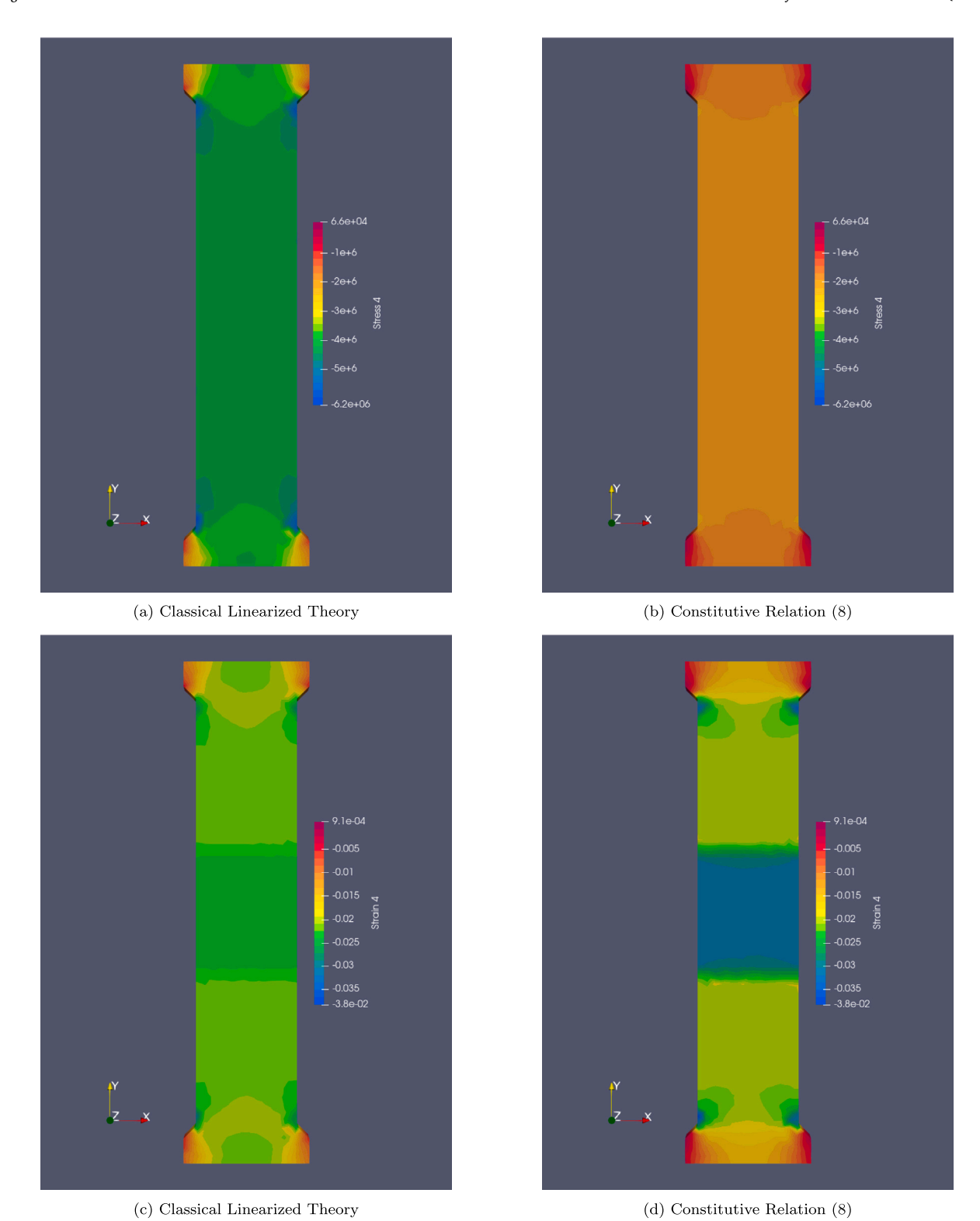
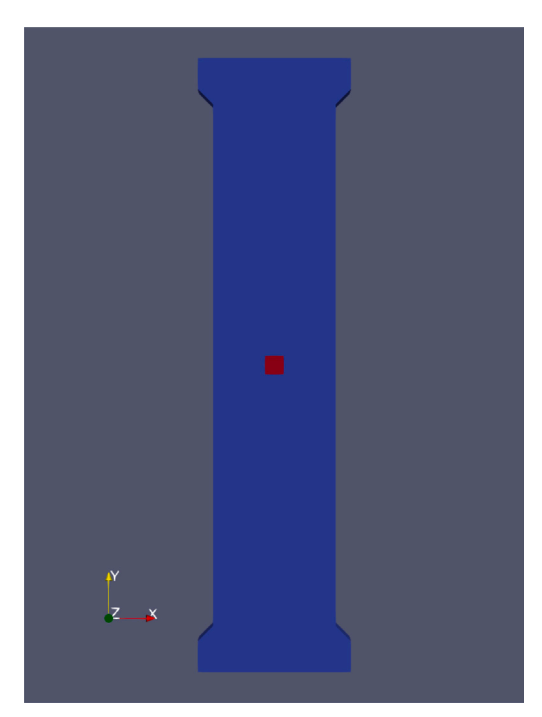


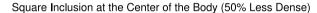
Fig. 6. Comparison of stress field  $\sigma_{yy}$  (top row) and  $\epsilon_{yy}$  (bottom row) for the two cases. The displacement field (prescribed boundary condition) is the same in both cases.

Figs. 5(b), 7(b), 9(b), 11(b), 13(b), 15(b), and 17(b) present a comparison between stresses and strains obtained for classical linearized theory and constitutive relation (8) for different cases. The spatial distribution of stresses and strains corresponding to when the maximum boundary displacements (applied equally for both the linearized and nonlinear cases) are imposed are shown in Figs. 6, 8, 10, 12, 14, 16, and 18.

For the chosen value of reference density changes in Table 2, stress concentration factors significantly differed between the linearized and nonlinear cases for the geometry with the hole and notch. Stress concentration factor is defined as the ratio between longitudinal stress  $(\sigma_{yy})$  near the hole and longitudinal stress  $(\sigma_{yy})$  at the far field. Stress concentration factor variations with respect to prescribed displacement at the boundary are shown in Figs. 19(a) and 19(b).



(a) Less dense central square inclusion.



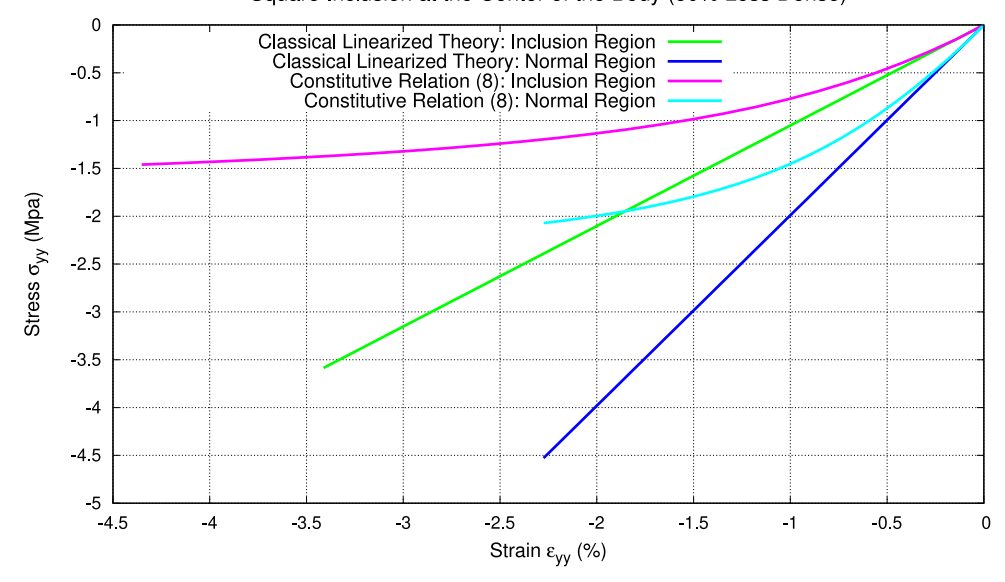


Fig. 7. Less dense central square inclusion.

- 4.2.1. Inhomogeneity in the center of the dogbone See Figs. 5 and 6.
- 4.2.2. Less dense central square inclusion in dogbone sample See Figs. 7 and 8.
- 4.2.3. Less dense lateral square inclusion in dogbone sample See Figs. 9 and 10.
- **4.2.4.** Denser circular inclusion in dogbone sample See Figs. 11 and 12.

- 4.2.5. Denser semi-circular lateral inclusion in dogbone sample See Figs. 13 and 14.
- 4.2.6. Dogbone sample with a central hole See Figs. 15 and 16.
- **4.2.7.** Dogbone sample with a semi-circular notch See Figs. 17–19.

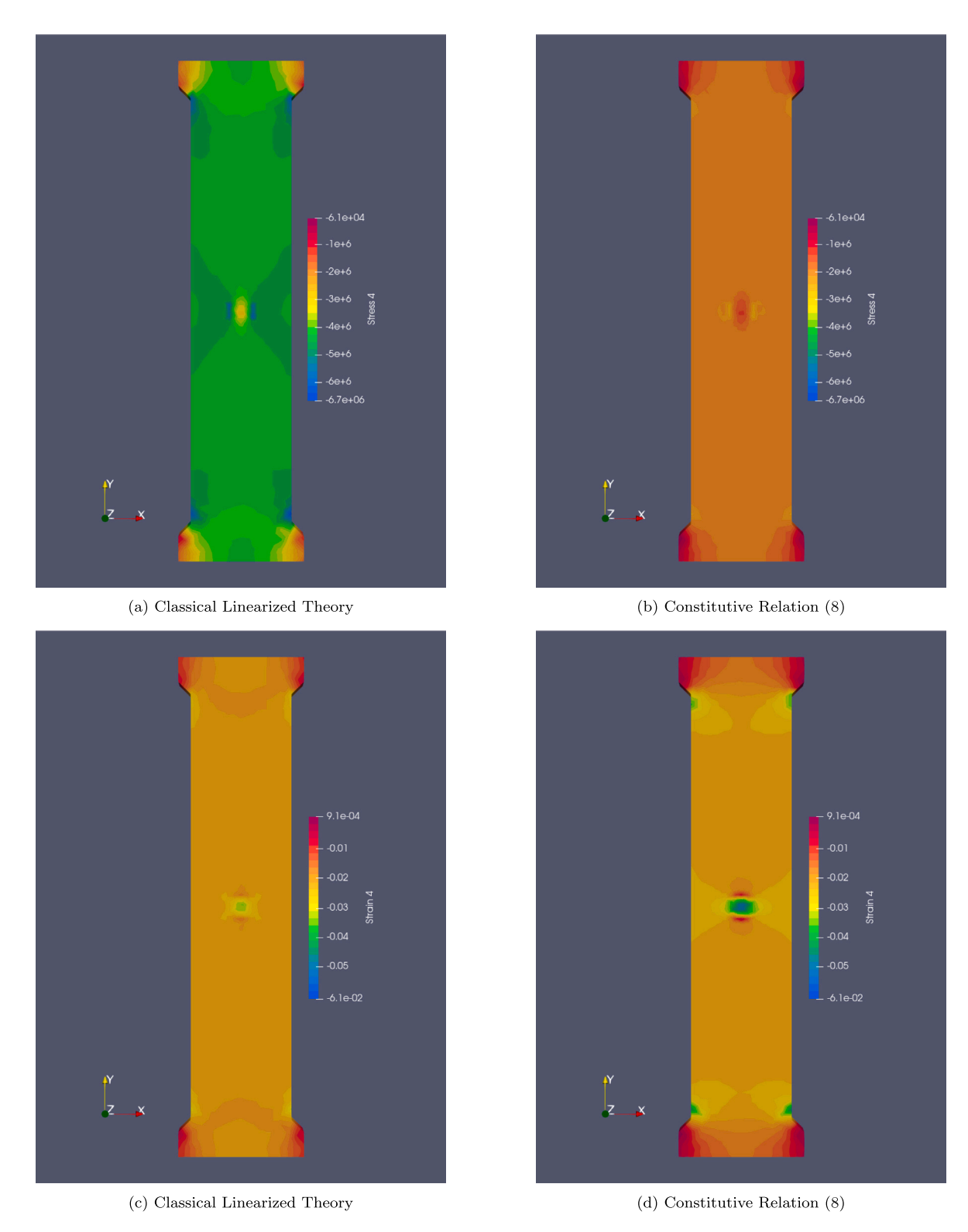
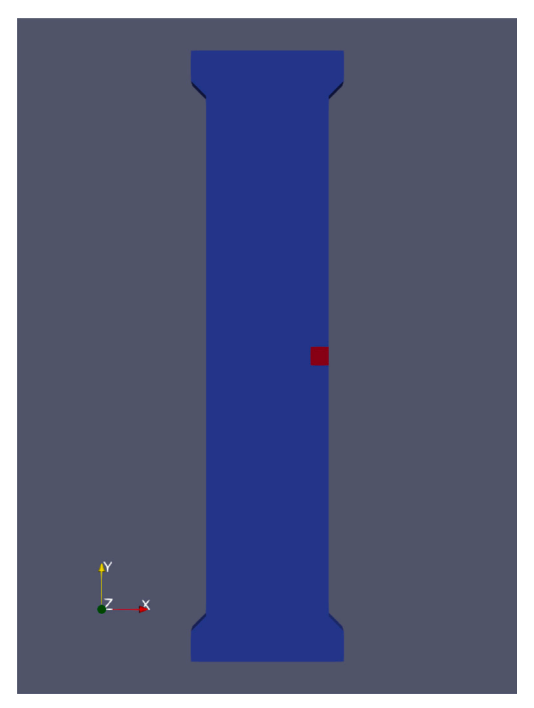


Fig. 8. Comparison of  $\sigma_{yy}$  (top row) and  $\epsilon_{yy}$  (bottom row) for the two cases. Prescribed displacement boundary condition is the same in both the cases.

# 5. Discussions and conclusions

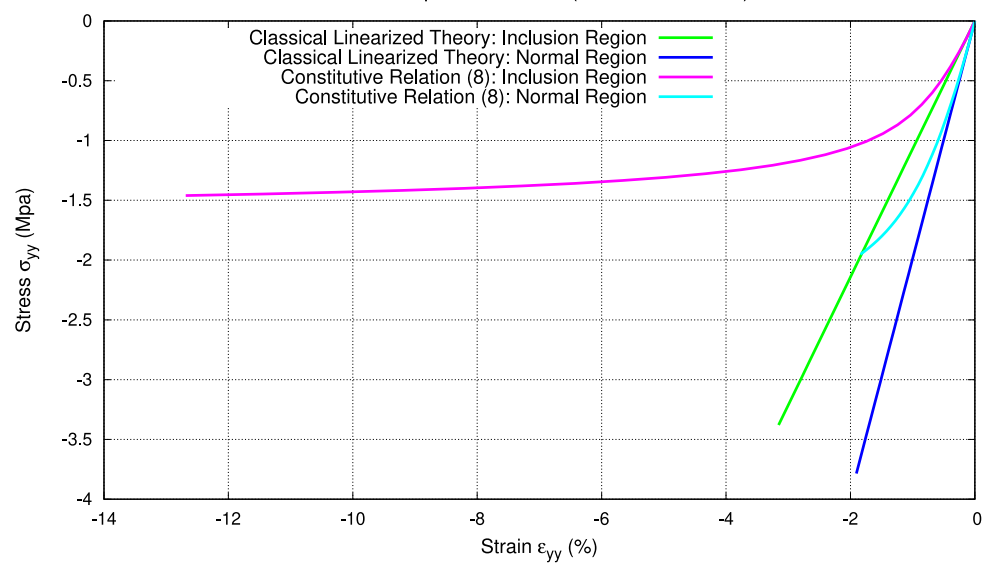
Our study reveals notable disparities in the prediction of the strains and the stresses between the linearized constitutive relation and our constitutive relation (8) for the bone. The constitutive relation we are employing is able to predict the response of trabecular bone in the

homogeneous dog bone sample much better than the linearized elastic constitutive relation. Since the linearized constitutive relation overpredicts the stress required by over 40% to produce a strain of around 2.5%, we would be making a serious error in thinking that the bone could take a lot higher load than it can for engendering the same strain.



(a) Less dense lateral square inclusion.

#### Lateral Square Inclusion (50% Less Dense)



(b) Comparison of results between the linearized elastic body and the body described by constitutive relation (8).

Fig. 9. Less dense lateral square inclusion.

The study underscores the importance of capturing nonlinearity exhibited by trabecular bone, accurately. In orthopedic applications, strains typically remain below 3%, and thus one might overlook the effects of nonlinearity in the response of the body and incorrectly conclude that the linearized elastic constitutive relation ought to apply. However, our findings emphasize the significance of considering nonlinear behavior even at these low strain levels. Although lower stresses in the nonlinear material may initially seem advantageous in terms of factors of safety in design and analysis, it is important to note that this aspect has potential drawbacks. For instance, lower stresses can

exacerbate stress shielding in orthopedic implants, leading to adverse physiological effects such as bone atrophy.

Furthermore, variations in mechanical properties, such as the modulus, resulting from differences in reference density can also significantly influence the state of stress and strain in the bone. In our study, we used data from just one experiment to determine the material properties of the bone. In order for us to have sufficient faith in the applicability of the constitutive relation, it is imperative for us to fit the predictions of our constitutive relation vis-a-vis other experimental data.

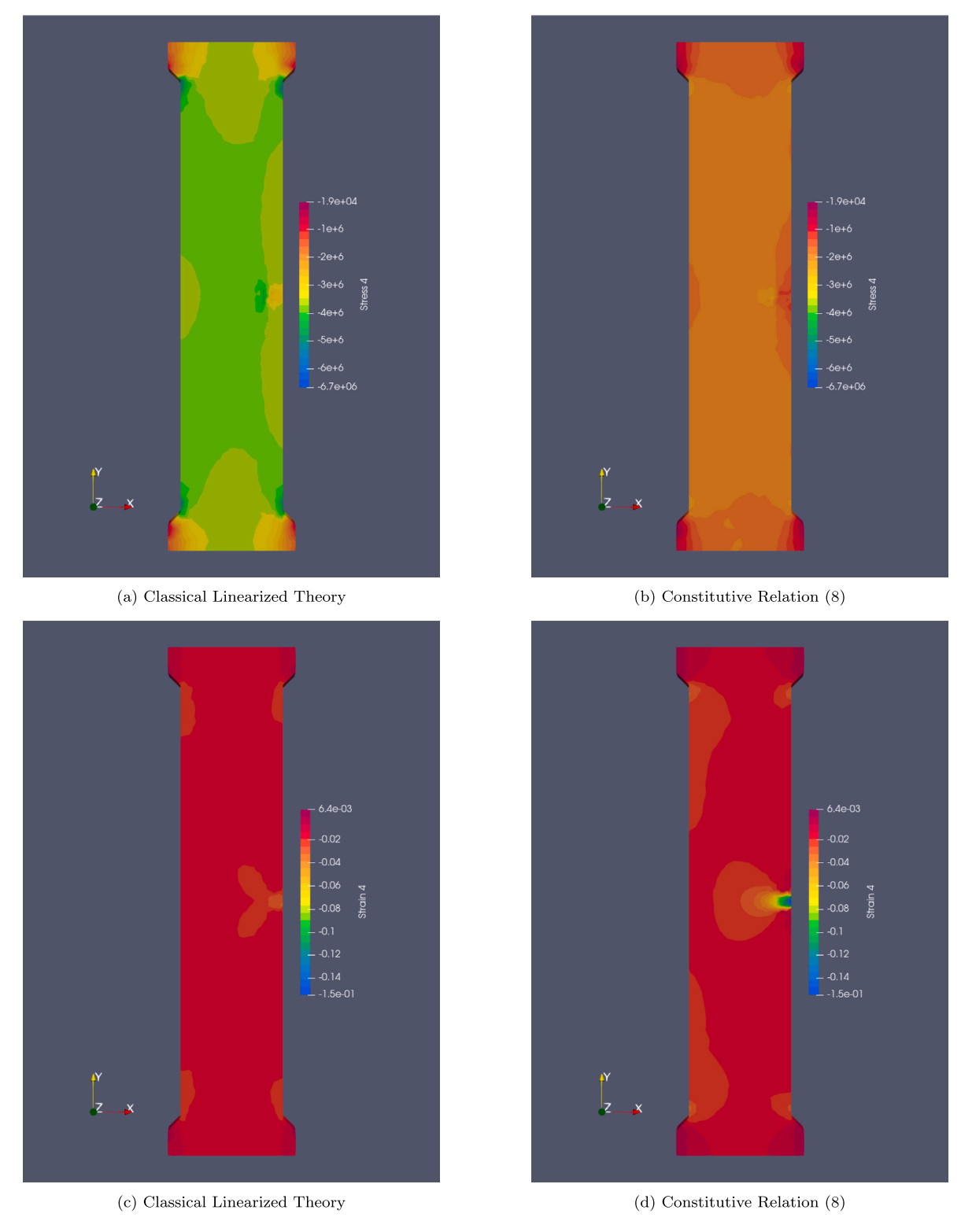
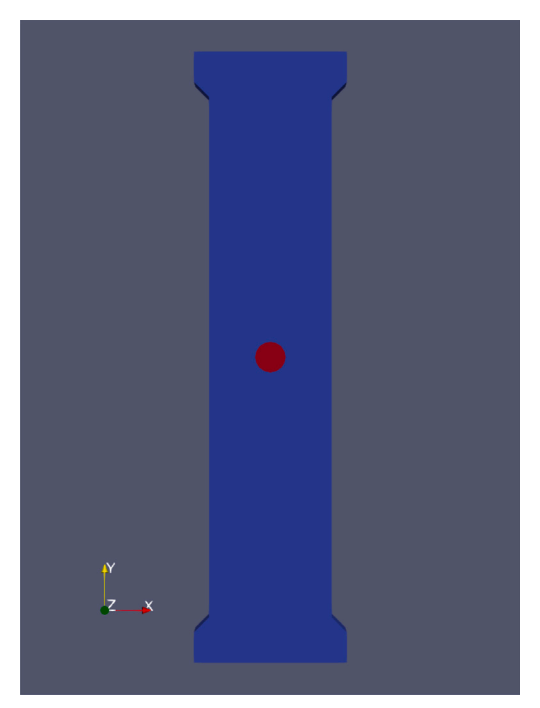


Fig. 10. Comparison of  $\sigma_{yy}$  (top row) and  $\epsilon_{yy}$  (bottom row) for the two cases. Prescribed displacement boundary condition is the same in both the cases.

0

-6 L -2.5

-2



(a) Denser circular inclusion.

Central Circular Inclusion with 50% Higher Density

# Classical Linearized Theory: Inclusion Region Classical Linearized Theory: Normal Region Constitutive Relation (8): Inclusion Region Constitutive Relation (8): Normal Region -1 -2 Stress o<sub>yy</sub> (Mpa) -3 -5

(b) Comparison of results between the linearized elastic body and the body described by constitutive relation (8).

Strain  $\epsilon_{yy}$  (%)

-0.5

0

-1.5

Fig. 11. Dogbone Sample with a denser circular inclusion.

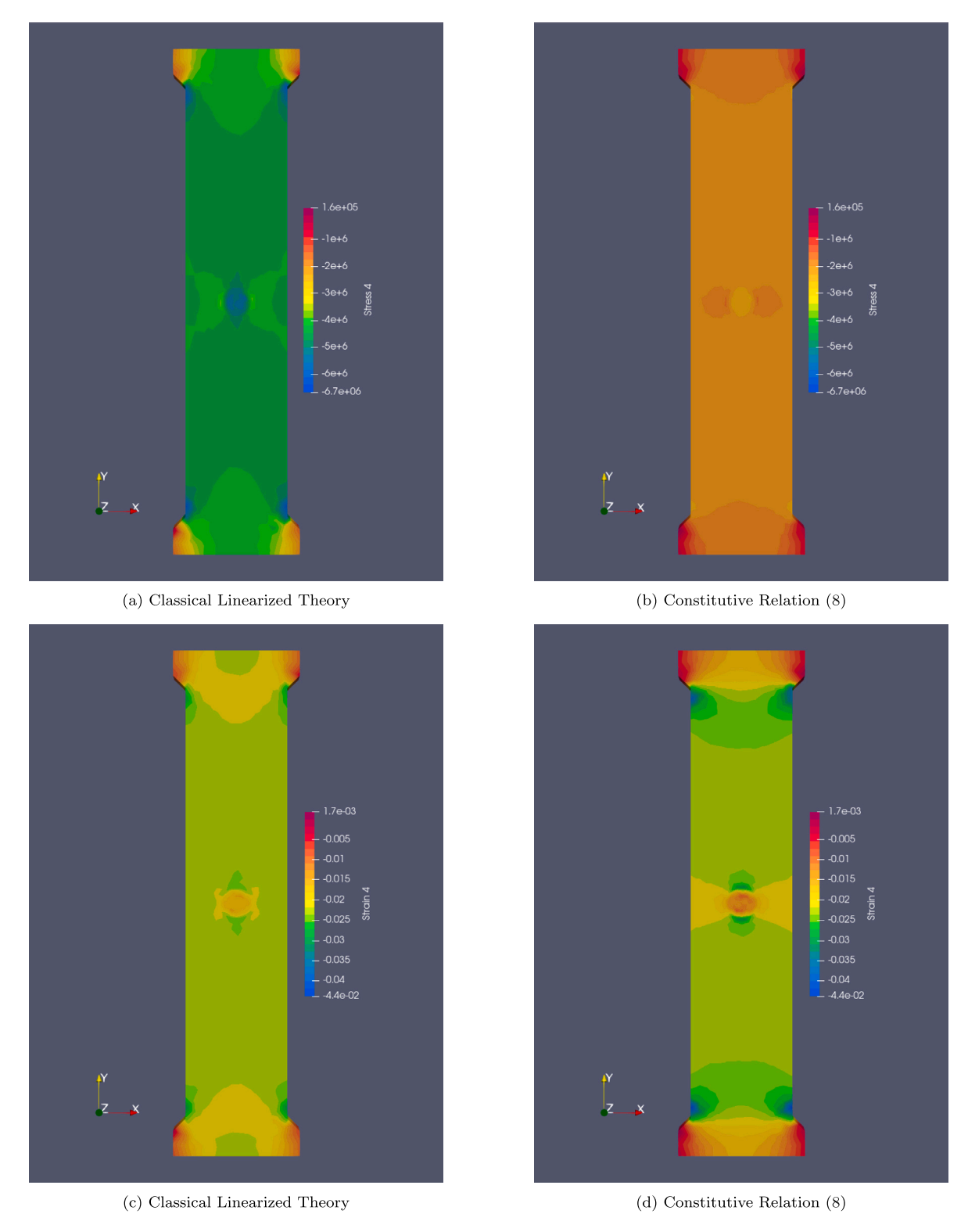
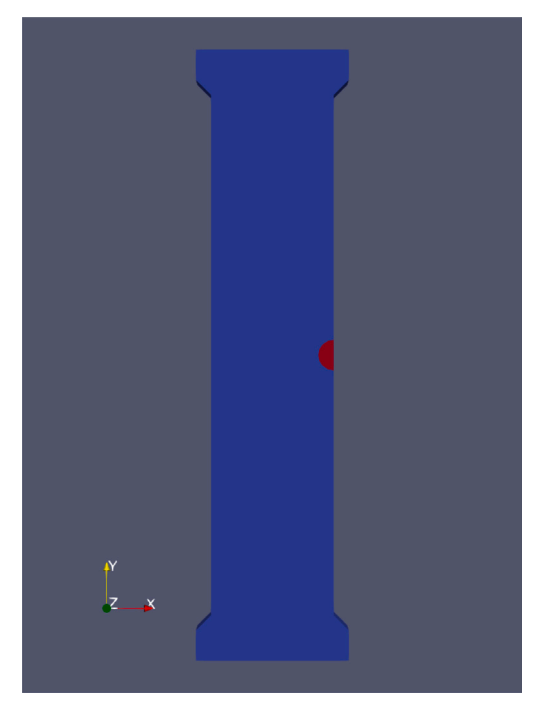


Fig. 12. Comparison of  $\sigma_{yy}$  (top row) and  $\epsilon_{yy}$  (bottom row) for the two cases. Prescribed displacement boundary condition is the same in both the cases.



(a) Denser semi-circular lateral inclusion.

# 0 Classical Linearized Theory: Inclusion Region Classical Linearized Theory: Normal Region Constitutive Relation (8): Inclusion Region Constitutive Relation (8): Normal Region -0.5 -1 -1.5 Stress o<sub>yy</sub> (Mpa) -2 -2.5 -3 -3.5 -4 -4.5 **-**5 -1.5 -0.5 -2.5 0 Strain $\epsilon_{yy}$ (%)

Denser Semi-circular Region with 50% Higher Density

 $\textbf{Fig. 13.} \ \ \textbf{Dogbone Sample with a denser semi-circular lateral inclusion}.$ 

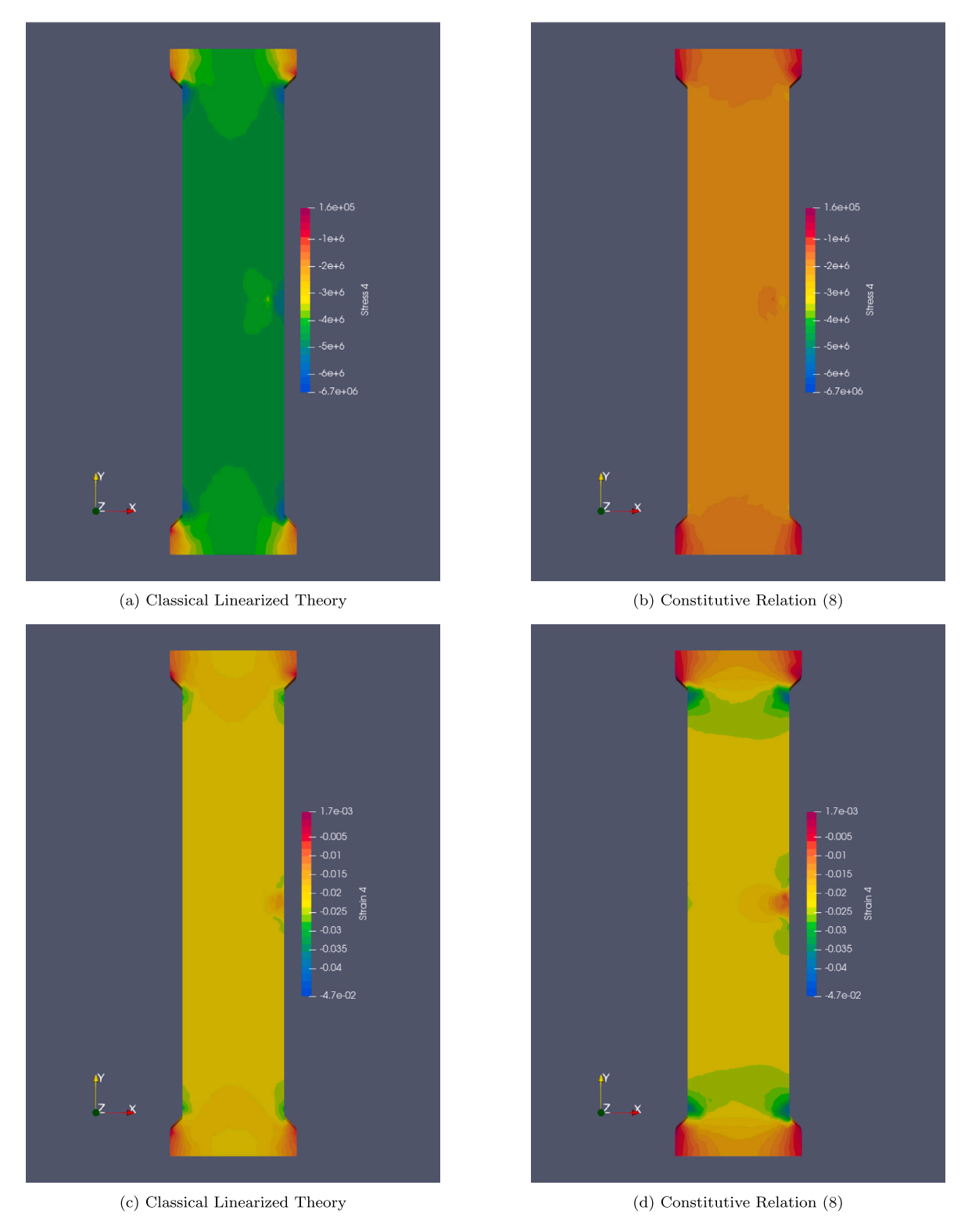
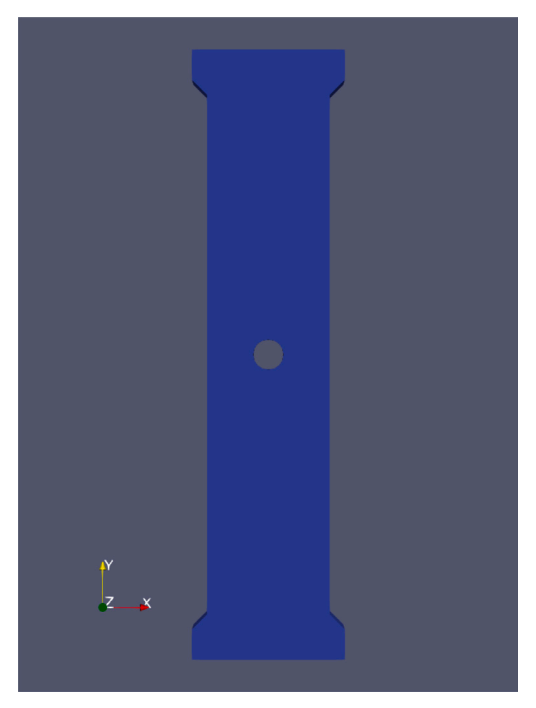


Fig. 14. Comparison of  $\sigma_{yy}$  (top row) and  $\epsilon_{yy}$  (bottom row) for the two cases. Prescribed displacement boundary condition is the same in both the cases.



(a) Geometry with a central hole.

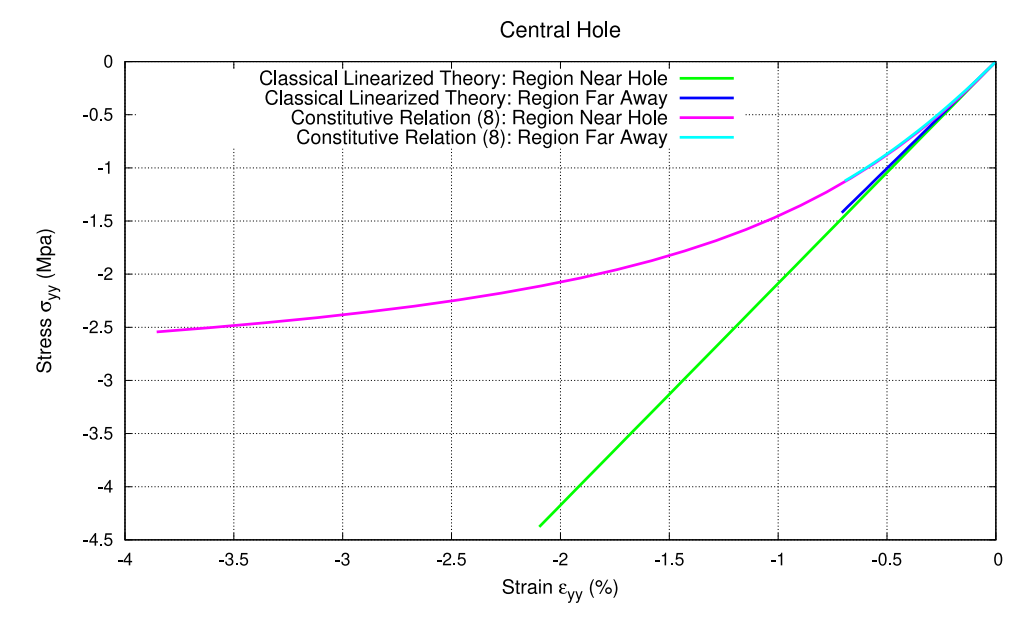


Fig. 15. Dogbone sample with a central hole.

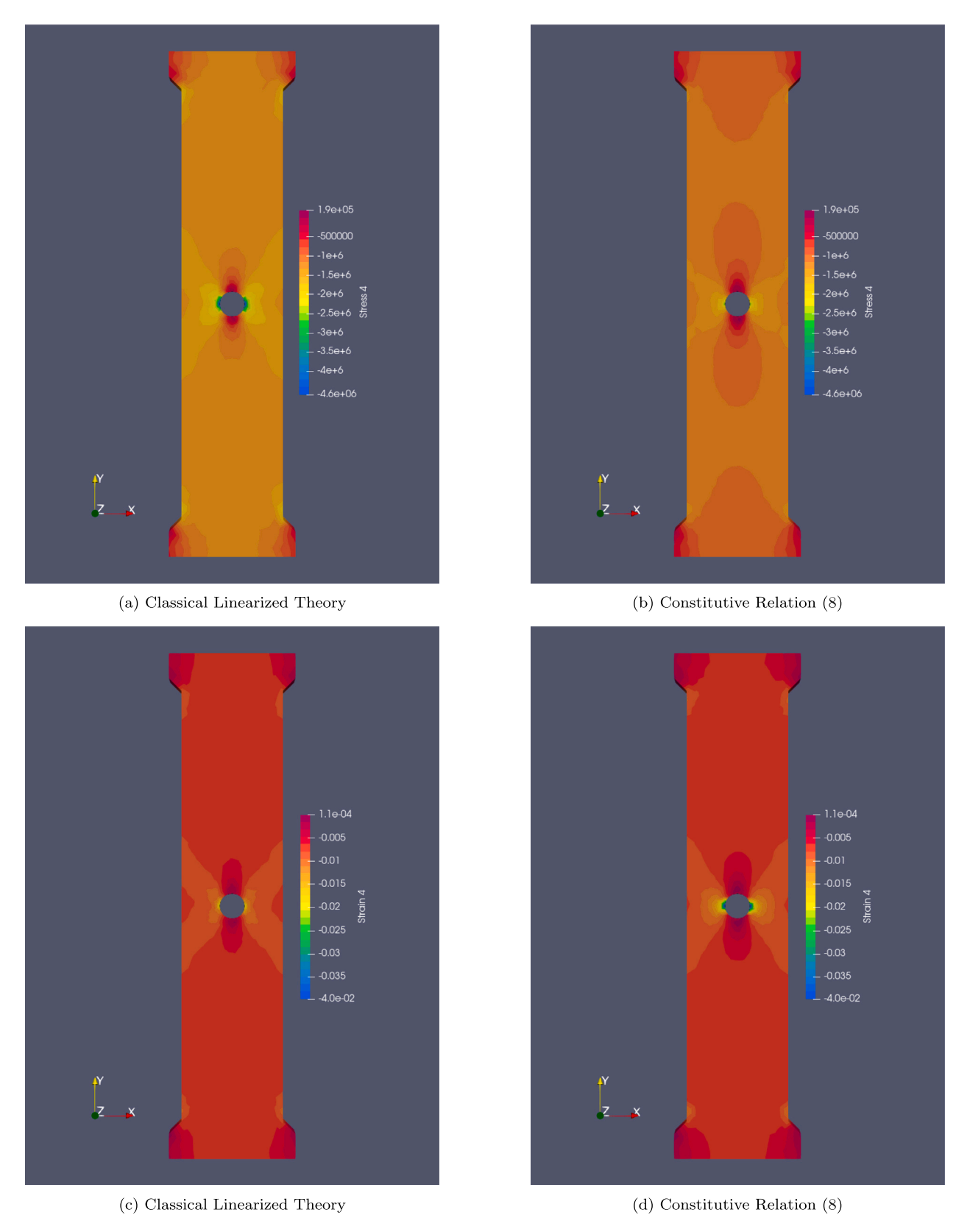
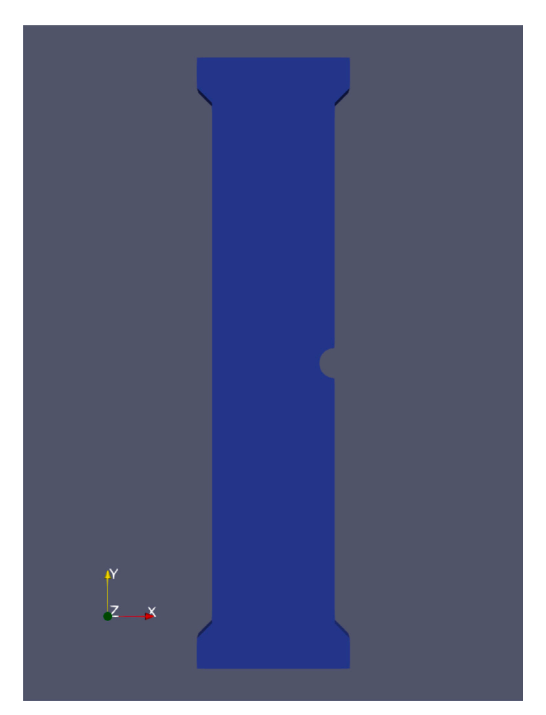


Fig. 16. Comparison of stress field  $\sigma_{yy}$  (top row) and  $\epsilon_{yy}$  (bottom row) for the two cases. Prescribed displacement boundary condition is the same in both the cases.



(a) Geometry with a semi-circular notch.

# Lateral Semi-Circular Notch 0 Classical Linearized Theory: Region Near Hole Classical Linearized Theory: Region Far Away Constitutive Relation (8): Region Near Hole Constitutive Relation (8): Region Far Away -0.5 -1 -1.5 Stress o<sub>yy</sub> (Mpa) -2 -2.5 -3 -3.5 -4 -4.5 **-**5 -2 -6 0 Strain $\epsilon_{yy}$ (%)

(b) Comparison of results between the linearized elastic body and the body described by constitutive relation (8).

 $\textbf{Fig. 17.} \ \ \textbf{Geometry with a semi-circular notch.}$ 

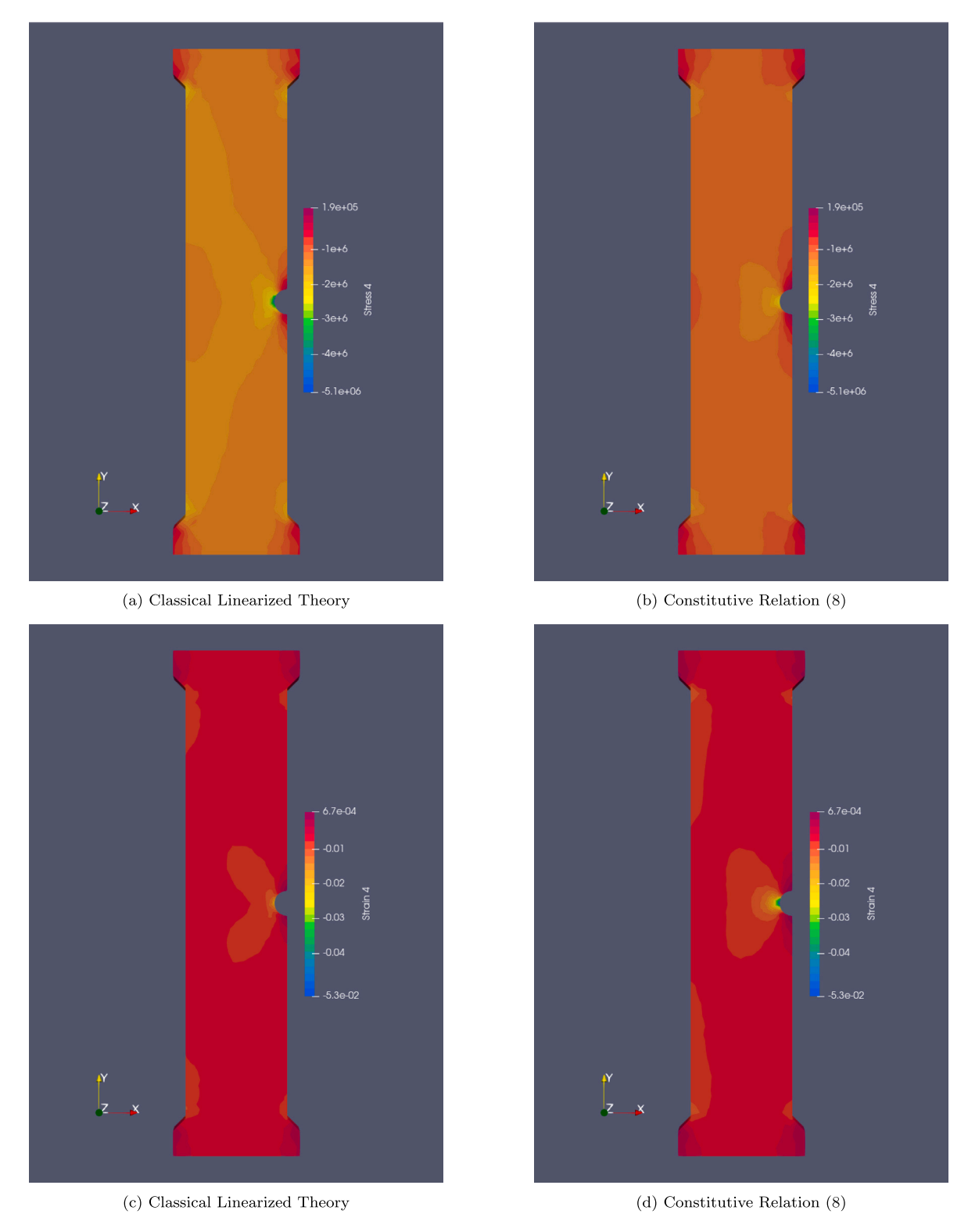
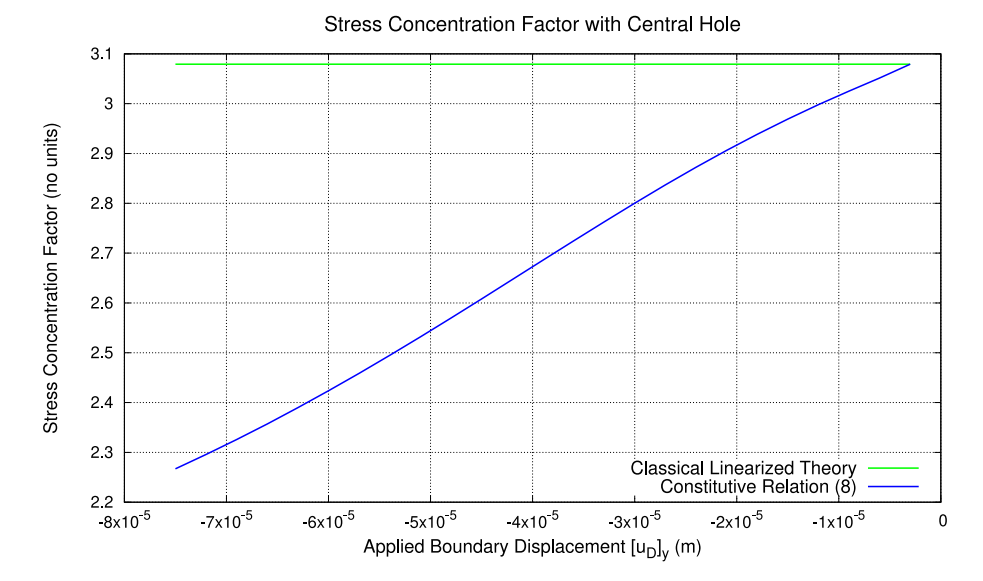
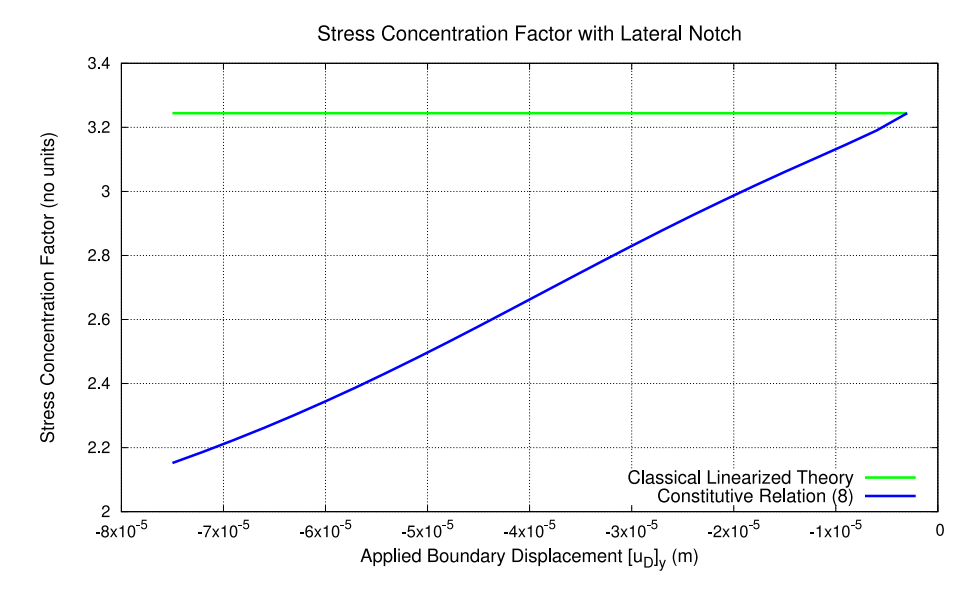


Fig. 18. Comparison of stress field  $\sigma_{yy}$  (top row) and  $\epsilon_{yy}$  (bottom row) for the two cases. Prescribed displacement boundary condition is the same in both the cases.



(a) Geometry with a central hole.



(b) Geometry with a semi-circular notch.

Fig. 19. Stress concentration factor.

# CRediT authorship contribution statement

J. Arumugam: Data curation, Formal analysis, Investigation, Writing – original draft. P. Alagappan: Formal analysis, Investigation, Methodology, Writing – original draft. J. Bird: Investigation, Writing – original draft. M. Moreno: Investigation, Writing – original draft. K.R. Rajagopal: Conceptualization, Investigation, Methodology, Supervision.

## Declaration of competing interest

The authors declare that they have no known competing financial interests or personal relationships that could have appeared to influence the work reported in this paper.

#### Data availability

No data was used for the research described in the article.

# Acknowledgments

KRR thanks the Office of Naval Research and the National Science Foundation, USA for its support of this research. KRR dedicates this paper to Giuseppe Saccomandi, a staunch friend and trustworthy collaborator.

## References

- M.B. Schaffler, D.B. Burr, Stiffness of compact bone: Effects of porosity and density, J. Biomech. 21 (1) (1988) 13–16.
- [2] R.W. McCalden, J.A. McGeough, M.B. Barker, et al., Age-related changes in the tensile properties of cortical bone. The relative importance of changes in porosity, mineralization, and microstructure, J. Bone Joint Surg. 75 (8) (1993) 1193–1205.
- [3] K. Bell, N. Loveridge, J. Power, N. Garrahan, B. Meggitt, J. Reeve, Regional differences in cortical porosity in the fractured femoral neck, Bone 24 (1) (1999) 57–64.
- [4] B. Helgason, E. Perilli, E. Schileo, F. Taddei, S. Brynjólfsson, M. Viceconti, Mathematical relationships between bone density and mechanical properties: A literature review, Clin. Biomech. 23 (2) (2008) 135–146.

- [5] M. Vanleene, C. Rey, M.-C.H.B. Tho, Relationships between density and Young's modulus with microporosity and physico-chemical properties of wistar rat cortical bone from growth to senescence, Med. Eng. Phys. 30 (8) (2008) 1049–1056
- [6] L. Cardoso, S.P. Fritton, G. Gailani, M. Benalla, S.C. Cowin, Advances in assessment of bone porosity, permeability and interstitial fluid flow, J. Biomech. 46 (2) (2013) 253–265.
- [7] R.S. Lakes, J.L. Katz, S.S. Sternstein, Viscoelastic properties of wet cortical bone—I. Torsional and biaxial studies, J. Biomech. 12 (9) (1979) 657–678.
- [8] T. Gottesman, Z. Hashin, Analysis of viscoelastic behaviour of bones on the basis of microstructure, J. Biomech. 13 (2) (1980) 89–96.
- [9] T. Iyo, Y. Maki, N. Sasaki, M. Nakata, Anisotropic viscoelastic properties of cortical bone, J. Biomech. 37 (9) (2004) 1433–1437.
- [10] Z. Wu, T.C. Ovaert, G.L. Niebur, Viscoelastic properties of human cortical bone tissue depend on gender and elastic modulus, J. Orthop. Res. 30 (5) (2012) 693–699.
- [11] M.E. Kersh, P.K. Zysset, D.H. Pahr, U. Wolfram, D. Larsson, M.G. Pandy, Measure-ment of structural anisotropy in femoral trabecular bone using clinical-resolution CT images, J. Biomech. 46 (15) (2013) 2659–2666.
- [12] D. Larsson, B. Luisier, M.E. Kersh, E. Dall'Ara, P.K. Zysset, M.G. Pandy, D.H. Pahr, Assessment of transverse isotropy in clinical-level CT images of trabecular bone using the gradient structure tensor, Ann. Biomed. Eng. 42 (2014) 950–959.
- [13] R.A. Yassine, R.F. Hamade, Transversely isotropic and isotropic material considerations in determining the mechanical response of geometrically accurate bovine Tibia bone, Med. Biol. Eng. Comput. 57 (2019) 2159–2178.
- [14] H.S. Hosseini, G. Maquer, P.K. Zysset, μCT-based trabecular anisotropy can be reproducibly computed from HR-pQCT scans using the triangulated bone surface, Bone 97 (2017) 114–120.
- [15] X.N. Dong, X.E. Guo, The dependence of transversely isotropic elasticity of human femoral cortical bone on porosity. J. Biomech. 37 (8) (2004) 1281–1287.
- [16] E.F. Morgan, O.C. Yeh, W.C. Chang, T.M. Keaveny, Nonlinear behavior of trabecular bone at small strains, J. Biomech. Eng. 123 (1) (2001) 1–9.
- [17] F. Taddei, M. Viceconti, M. Manfrini, A. Toni, Mechanical strength of a femoral reconstruction in paediatric oncology: A finite element study, Proc. Inst. Mech. Eng. Part H: J. Eng. Med. 217 (2) (2003) 111–119.
- [18] Y.-Y. Hsieh, F.-Y. Tsuang, Y.-J. Kuo, C.-H. Chen, C.-J. Chiang, C.-L. Lin, Biomechanical analysis of single-level interbody fusion with different internal fixation rod materials: A finite element analysis, BMC Musculoskeletal Disord. 21 (2020) 1–9.
- [19] T. Khurelbaatar, K. Kim, Y. Hyuk Kim, A cervico-thoraco-lumbar multibody dynamic model for the estimation of joint loads and muscle forces, J. Biomech. Eng. 137 (11) (2015) 111001.
- [20] F. Eggermont, L. Derikx, N. Verdonschot, I. Van Der Geest, M. De Jong, A. Snyers, Y. Van Der Linden, E. Tanck, Can patient-specific finite element models better predict fractures in metastatic bone disease than experienced clinicians?: Towards computational modelling in daily clinical practice, Bone Joint Res. 7 (6) (2018) 430–439.
- [21] M. Wang, N. Yang, X. Wang, A review of computational models of bone fracture healing, Med. Biol. Eng. Comput. 55 (2017) 1895–1914.
- [22] B. Haimson, T. Tharp, Stresses around boreholes in bilinear elastic rock, Soc. Petrol. Eng. J. 14 (02) (1974) 145–151.
- [23] K. Fuenkajorn, S. Klanphumeesri, Direct tension tests of intact rocks using compression-to-tension load converter, Eng. J. Res. Dev. 21 (2) (2010) 51–57.
- [24] S. Patel, C.D. Martin, Evaluation of tensile young's modulus and Poisson's ratio of a bi-modular rock from the displacement measurements in a Brazilian test, Rock Mech. Rock Eng. 51 (2) (2018) 361–373.
- [25] P. Sundaram, J. Corrales, Brazilian tensile strength of rocks with different elastic properties in tension and compression, Int. J. Rock Mech. Min. Sci. Geomech. Abstr:(United States) 17 (2) (1980).
- [26] P. Johnson, P. Rasolofosaon, Manifestation of nonlinear elasticity in rock: Convincing evidence over large frequency and strain intervals from laboratory studies, Nonlinear Process. Geophys. 3 (2) (1996) 77–88.

- [27] R. Bustamante, C. Ortiz, A bimodular nonlinear constitutive equation for rock, Appl. Eng. Sci. 8 (2021) 100067.
- [28] A. Cauchy, Recherches sur L'ÉQuilibre Et Le Mouvement IntÉRieur Des Corps Solides Ou Fluides, ÉLastiques Ou Non ÉLastiques, 1823.
- [29] A. Cauchy, Sur les équations qui expriment les conditions d'équilibre ou les lois du mouvement intérieur d'un corps solide, élastique ou non élastique, Ex. de Math. 3 (1828) 160–187.
- [30] G. Green, On the laws of the reflexion and refraction of light at the common surface of two non-crystallized media, Trans. Cambridge Philos. Soc. (1837) (1838).
- [31] K.R. Rajagopal, An implicit constitutive relation for describing the small strain response of porous elastic solids whose material moduli are dependent on the density. Math. Mech. Solids 26 (8) (2021) 1138–1146.
- [32] K.R. Rajagopal, On implicit constitutive theories, Appl. Math. 48 (2003) 279-319.
- [33] K.R. Rajagopal, A note on the linearization of the constitutive relations of non-linear elastic bodies, Mech. Res. Commun. 93 (2018) 132–137.
- [34] K.R. Rajagopal, The elasticity of elasticity, Zeitschrift f
  ür angew. Math. Phys. 58 (2007) 309–317.
- [35] K.R. Rajagopal, Conspectus of concepts of elasticity, Math. Mech. Solids 16 (5) (2011) 536–562.
- [36] V. Prusa, K.R. Rajagopal, A. Wineman, Pure bending of an elastic prismatic beam made of a material with density-dependent material parameters, Math. Mech. Solids 27 (8) (2022) 1546–1558.
- [37] K.R. Rajagopal, Remarks on the notion of "pressure", Int. J. Non-linear Mech. 71 (2015) 165–172.
- [38] P.T. Murru, K.R. Rajagopal, Stress concentration due to the presence of a hole within the context of elastic bodies, Mater. Des. Process. Commun. 3 (5) (2021) e219.
- [39] P.T. Murru, K.R. Rajagopal, Stress concentration due to the bi-axial deformation of a plate of a porous elastic body with a hole, ZAMM-J. Appl. Math. Mech. /Zeitschrift für Angew. Math. Mech. 101 (11) (2021) e202100103.
- [40] B. Vajipeyajula, P.T. Murru, K.R. Rajagopal, Stress concentration due to an elliptic hole in a porous elastic plate, Math. Mech. Solids 28 (3) (2023) 854–869.
- [41] B. Vajipeyajula, P.T. Murru, K.R. Rajagopal, Stress concentration due to the presence of a rigid elliptical inclusion in porous elastic solids described by a new class of constitutive relations, J. Elasticity (2023) 1–19.
- [42] H. Itou, V.A. Kovtunenko, K.R. Rajagopal, On an implicit model linear in both stress and strain to describe the response of porous solids, J. Elasticity 144 (1) (2021) 107–118.
- [43] H. Itou, V.A. Kovtunenko, K.R. Rajagopal, Investigation of implicit constitutive relations in which both the stress and strain appear linearly, adjacent to non-penetrating cracks, Math. Models Methods Appl. Sci. 32 (07) (2022) 1475–1492.
- [44] B. Erbaş, J. Kaplunov, K.R. Rajagopal, 2D asymptotic analysis of a thin elastic beam with density-dependent generalized Young's modulus, in: Mechanics of Heterogeneous Materials, Springer, 2023, pp. 501–513.
- [45] L. Røhl, E. Larsen, F. Linde, A. Odgaard, J. Jørgensen, Tensile and compressive properties of cancellous bone, J. Biomech. 24 (12) (1991) 1143–1149.
- [46] V. Prusa, L. Trnka, Mechanical response of elastic materials with density dependent Young modulus, Appl. Eng. Sci. 14 (2023) 100126.
- [47] T.M. Keaveny, Mechanistic approaches to analysis of trabecular bone, Forma 12 (3) (1998) 267–275.
- [48] T.M. Keaveny, E.F. Morgan, G.L. Niebur, O.C. Yeh, Biomechanics of trabecular bone, Annu. Rev. Biomed. Eng. 3 (1) (2001) 307–333.
- [49] A. Logg, K.-A. Mardal, G. Wells, Automated Solution of Differential Equations By the Finite Element Method: The FEniCS Book, vol. 84, Springer Science & Business Media, 2012.
- [50] O. Zienkiewicz, P. Jain, E. Onate, Flow of solids during forming and extrusion: Some aspects of numerical solutions, Int. J. Solids Struct. 14 (1) (1978) 15–38.